



A Fast Rechargeable Lithium-Ion Battery at Subfreezing Temperatures

Chao-Yang Wang,^{a,b,*} Terrence Xu,^b Shanhai Ge,^b Guangsheng Zhang,^{a,*} Xiao-Guang Yang,^a and Yan Ji^b

^aDepartment of Mechanical & Nuclear Engineering and Electrochemical Engine Center (ECEC), The Pennsylvania State University, University Park, Pennsylvania 16802, USA

^bEC Power, State College, Pennsylvania 16803, USA

Widespread adoption of plug-in electric vehicles hinges upon fast rechargeability of lithium-ion batteries in all climates. To date, Li-ion batteries subject to quick charging in extreme cold grow lithium dendrites which consume cyclable lithium thus severely shortening battery life and compromise safety. Here we experimentally demonstrate 3C fast charging at -30°C for more than 500 cycles using a new cell structure, the all-climate battery (ACB). Addition of a metal foil creates immense internal heating in the ACB cell upon activation by short pulses of discharge and charge current, allowing charge to 80% state-of-charge in 14 min as opposed to 160 min for a conventional Li-ion cell. Moreover, the ACB cell withstands more than 500 fast-charge cycles while the conventional cell incurs 20% capacity loss after only 12 cycles. The experimental pouch cell of 10 Ah consists of a graphite anode and a NCM622 cathode with a nickel foil coated by polyethylene terephthalate as an internal heating element. We believe that the self-heating ACB cell with $11.4\times$ faster charging and $40\times$ better cycle life enables a ubiquitous, weather-independent fast-charging infrastructure required for affordable vehicle electrification free of range anxiety. This fast rechargeable battery at low temperatures is also essential for outdoor robots and drones as well as can substantially reduce battery size and cost for home and grid energy storage.

© The Author(s) 2016. Published by ECS. This is an open access article distributed under the terms of the Creative Commons Attribution 4.0 License (CC BY, <http://creativecommons.org/licenses/by/4.0/>), which permits unrestricted reuse of the work in any medium, provided the original work is properly cited. [DOI: 10.1149/2.0681609jes] All rights reserved.

Manuscript submitted May 4, 2016; revised manuscript received June 10, 2016. Published July 13, 2016.

Two major barriers to mainstream adoption of plug-in electric vehicles (PEVs) are high cost and short drive range of lithium-ion batteries.¹ A single solution to both is to deploy 100-mile PEVs powered by ~ 20 kWh batteries combined with 5–15 min fast-charging infrastructure. This broadens PEV affordability due to the use of small batteries on-board, and alleviates drive range anxiety thanks to expedient fast charging. Additionally, this approach facilitates proliferation of fast-charging infrastructure due to reduced charging power required for smaller batteries. For example, existing supercharge stations² of 120 kW and DC quick charging stations³ of 50 kW can readily charge 20 kWh batteries in 10 and 24 minutes, respectively. In a sense, the fast charging infrastructure acts as an off-board range extender which costs nothing to consumers while preserving vehicle's low energy consumption per mile and effectively eliminating range anxiety.

Widespread vehicle electrification requires a fast charging method that reaches 80% of state-of-charge (SOC) in minutes under all weather conditions. Unfortunately, Li-ion batteries are notoriously incapable of fast charging at subzero temperatures due to propensity of lithium to deposit on the graphite anode in dendritic structures.^{4–8} It is believed that during charging, Li plating on the graphite particle surface competes with Li intercalation into anode active-material particles; as such, Li plating preferentially occurs at high charge currents and/or low temperatures due to reduced intercalation kinetics of the anode. Other important factors affecting Li plating are anode active materials and electrolytes. For example, a graphite anode is more susceptible to Li plating than hard carbon due to the proximity of the former's equilibrium potential to Li. Electrolytes and additives to stabilize the solid-electrolyte interphase (SEI) layer, such as vinylene carbonate (VC), have been shown to significantly influence Li plating as they alter the charge-transfer and diffusion processes related to the Li intercalation kinetics of the anode.⁹ A major symptom of Li plating is drastic loss in capacity in addition to hazardous consequences. Indeed, recent data showed that 20% capacity is lost due to Li plating after only 90 cycles of 1C charge to 80% SOC of a 2.5 Ah graphite-LFP cell at -22°C .¹⁰ Similarly, Ouyang et al.¹¹ reported a loss of 25% capacity in an 11.5 Ah graphite-LFP cell after only 40 cycles of C/2 charge at -10°C .

In this paper we demonstrate, for the first time, 3C charging to 80% SOC from -30°C within 15 min for over 500 cycles without Li plating. This new fast-charge capability is made possible by a novel battery structure called all-climate battery (ACB), first proposed by Wang et al.¹² The ACB cell uses a metal foil to create immense internal heating prior to charging so as to greatly enhance Li intercalation kinetics in anodes by thermal stimulation of the electrode-electrolyte interface. Figure 1 shows this simple structure and working principle of an ACB cell where one tab of the metal foil is electrically connected to the negative terminal, being welded together with the tabs of all

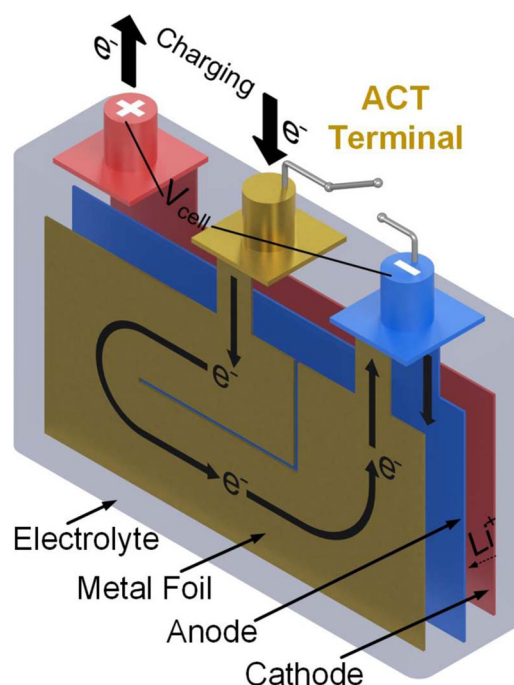


Figure 1. Schematic view and working principle of All-climate battery (ACB) in charging. A metal foil is inserted to self-heat inside the cell by turning the switch off during an activation period.

*Electrochemical Society Member.

^zE-mail: cxw31@psu.edu

anode layers. The other tab extends outside the cell to form a third terminal, the activation (ACT) terminal. Thus, in addition to positive and negative terminals, the ACB cell features a third ACT terminal used to activate battery internal heating from low temperatures prior to charging. A switch connects the ACT with the negative terminal and, when left open during the process of cell activation, forces electrons to flow through the metal foil (Figure 1) generating substantial ohmic heat to rapidly warm up the battery materials and electrochemical interfaces. Once the battery core reaches a temperature such as 10°C conducive to fast charging, the activation process is completed and battery charging begins. The switch between the ACT and negative terminal closes, causing electrons to bypass the metal foil and reverting the ACB cell to a conventional Li-ion cell with very low internal resistance and high charge acceptance. During ACB cell operation at room temperature, cell surface temperature controls the switch between ACT and negative terminals such that the switch remains closed. In this work, we demonstrate fast charging of Li-ion cells at very low temperatures, which has never been done before.

Experimental

We fabricate 10 Ah ACB pouch cells using NCM622 ($\text{LiNi}_{0.6}\text{Co}_{0.2}\text{Mn}_{0.2}\text{O}_2$) as cathodes and graphite (Nippon Carbon) as anodes with 1 M of LiPF_6 dissolved in EC/EMC (3:7 by wt.) + 2wt% VC as electrolyte. The capacity ratio of negative to positive electrode, or NP ratio, is designed at 1.2. The 10 Ah pouch cell contains a stack of 34 anode and 33 cathode layers. A Celgard-2325 separator of 25 μm in thickness is used. A nickel foil sized at 56 milli-Ohm is coated with a thin (28 μm) backing material of polyethylene terephthalate for electrical insulation and sandwiched between 2 single-sided anode layers. This 3-layer assembly is then stacked in the center of the cell. The cathodes are prepared by coating NMP based slurry onto 15 μm thick Al foil, whose dry material consists of NCM622 (91.5 wt%), Super-C65 (Timcal) (4.4 wt%) and PVdF (Hitachi) (4.1 wt%) as a binder. The anodes are prepared by coating deionized (DI) water-based slurry onto 10 μm thick Cu foil, whose dry material consists of graphite (95.4 wt%), Super-C65 (1.0 wt%), SBR (JSR) (2.2 wt%) and CMC (Nippon Paper) (1.4 wt%).

Each ACB pouch cell has a 152×75 mm footprint area, weighs 206 g, and has 10 Ah nominal capacity (relative to which all C-rates in this report are given) with specific energy of 172 Wh/kg and energy density of 334 Wh/L. The Ni foil we add in an ACB cell, weighs ~ 100 g per kWh battery and costs \$1/kWh based upon Nickel price of \$10/kg. Compared to the best specific energy of current Li-ion battery systems, i.e. 150 Wh/kg battery-system, and an assumed battery cost of \$250/kWh,¹³ the added weight and cost due to ACB technology are 1.5% and 0.4% of the baseline battery. Figure 2 displays the discharge/charge performance of the ACB cell without activation under various C-rates at different ambient temperatures.

An ACB cell initially at 20% SOC is soaked in an environmental chamber for over 3 hours to reach thermal equilibrium with the subfreezing ambient. Prior to battery charging at a subzero temperature, a pulse activation is first carried out where the cell voltage is pulsed between 4.2 V for one second with the charge current limited at 3C and 2.1 V for one second with the discharge current capped at 5C. The pulse activation is completed when the cell's outer surface temperature is detected to reach 10°C. Subsequently, the ACB cell is subject to 3C charging with 4.2 V voltage limit until either 80% SOC or C/20 is reached. The end SOC value of 80% is commonly used in DC fast-charging applications. Because battery activation is integral to fast charging for ACB cells, the total charge time in this work is always referred to as the sum of activation and charging periods. For comparison, a baseline cell without Ni foil is tested with the same charge protocol: 3C, 4.2 V, and 80% SOC or C/20 cutoff. For cycling tests, the cell charged at 80% SOC rests for 5 minutes, followed by 1C discharge back to 20% SOC and rest at open circuit and soaking in the -30°C environment chamber for 2–3 hours to reach complete thermal equilibrium with the ambient. Thus each charging cycle for ACB cells consists of four stages: pulse activation, 3C charging to 80% SOC, 1C

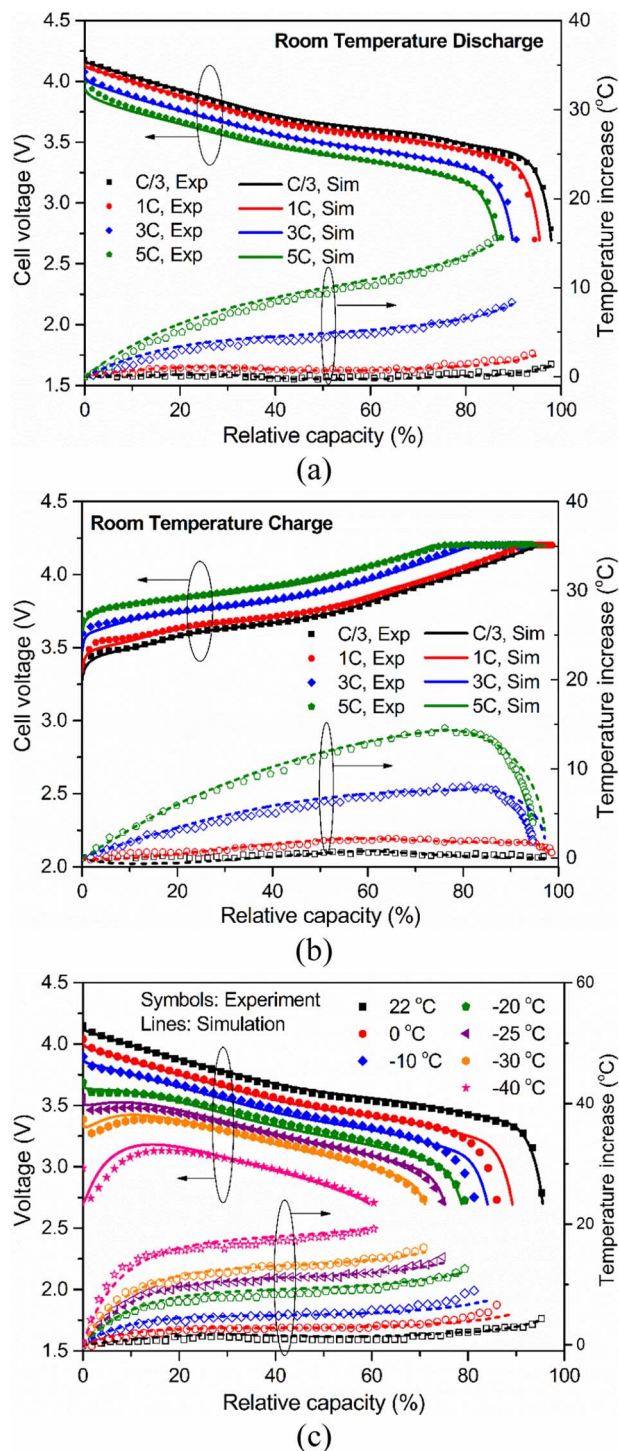


Figure 2. Discharge and charge performance of the 10 Ah ACB cell at various C-rates and temperatures, and comparison of predicted (lines) and measured (symbols) voltage and temperature curves for: (a) room-temperature discharge, (b) room-temperature charge, (c) 1C discharge at various ambient temperatures.

discharge back down to 20% SOC, and rest and cool-down to return cell temperature to the ambient temperature.

Electrochemical-Thermal Coupled Simulation

Electrochemical-thermal coupled modelling of an ACB cell is carried out with a commercial simulation package – AutoLion 1D.^{14–16}

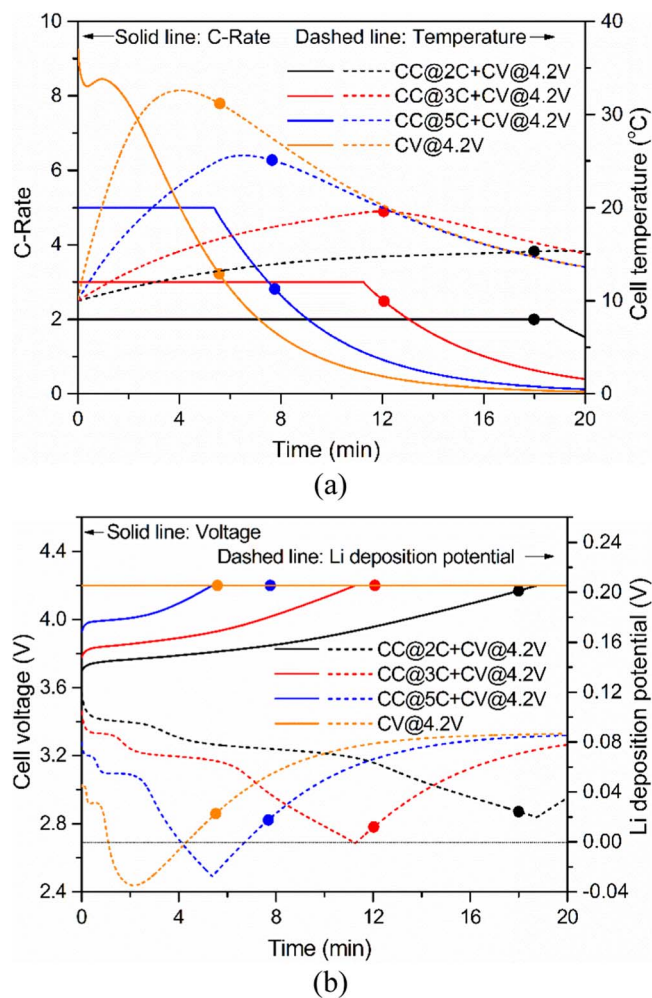


Figure 3. Simulation results of various fast charging protocols from 10°C. (a) Charge current and cell temperature. (b) Cell voltage and Li deposition potential at the anode-separator interface. The highest charge current is 3C without making the Li deposition potential turn negative, marking the onset of Li plating. Dots in the figures correspond to 80% SOC.

Electrochemical and transport properties of the graphite anode and the electrolyte are taken either from the material database built into the AutoLion package or from Ref. 8. The properties of NCM622 cathode material, such as the solid-state diffusivity and exchange current density, over a range of temperature -30 to 60°C and electrolyte concentration 0 to 4 M, are obtained from the experimental measurements of Leng and Wang.¹⁷ The heat transfer coefficient from the cell surface to the ambient is set at 20 W/m²K in all simulations. The customized simulation model for the present ACB cell is first validated against experimental data of cell voltage and temperature profiles in both discharge and charge over a wide range of C-rates and ambient temperatures, as shown in Figures 2a–2c.

The experimentally validated model for ACB cells, in AutoLion 1D, is then used to estimate Li deposition potential along with cell voltage, charging current and cell temperature in various charging protocols. Here, Li deposition potential is defined as the difference between the electronic and electrolyte phases further subtracting the ohmic loss across the solid-electrolyte interphase (SEI) layer, i.e. $(\phi_s - \phi_e - I^* R_{\text{SEI}})$, where I and R_{SEI} are the solid-phase current density and SEI resistance evaluated locally at the anode-separator interface in a cell. Due to zero equilibrium potential of Li plating, a negative value of the Li deposition potential signals the onset of Li plating in a cell. Figure 3 shows the simulation results for four charging scenarios from 10°C: 2C, 3C and 5C CCCV charging (capped at

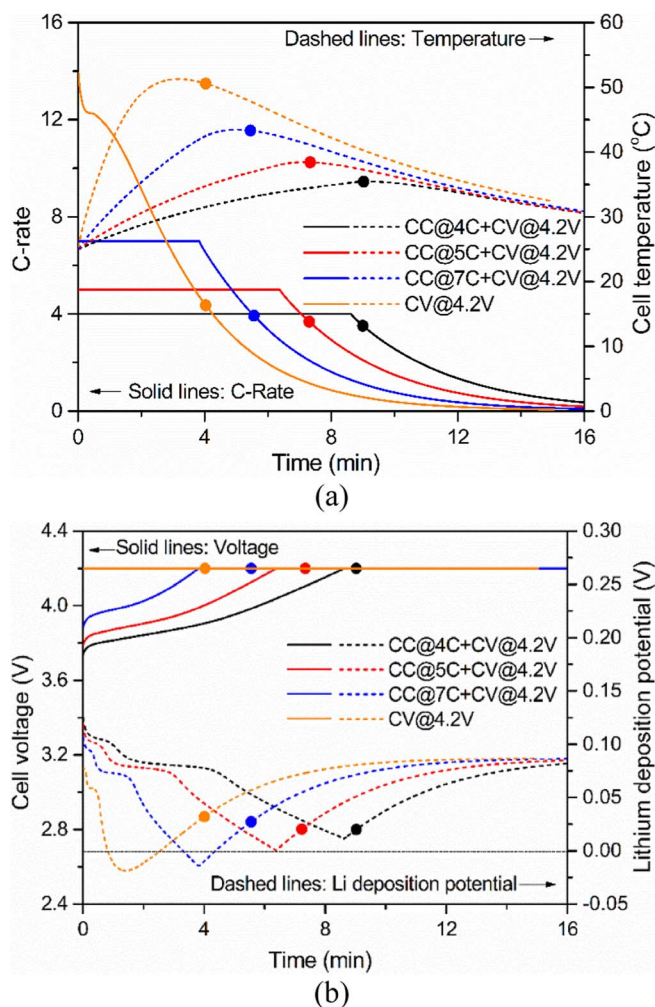


Figure 4. Simulation results of various fast charging protocols from 25°C. (a) Charge current and cell temperature. (b) Cell voltage and Li deposition potential at the anode-separator interface. The highest charge current is 5C without making the Li deposition potential turn negative, marking the onset of Li plating. Dots in the figures correspond to 80% SOC.

4.2 V), and the 4.2 V constant voltage charging. The CV charging is most aggressive. Notice that the predicted Li deposition potential curves during CCCV charging strongly resemble the experimentally measured ones of Ratnakumar and Smart,⁹ in that they are dropping along the CC period, reach minimal points at the transition from CC to CV phase, and subsequently rise along the CV period. It can be seen from Figure 3b that 3C CCCV charging is the fastest without making the Li deposition potential turn negative. Both 5C and 4.2 V CV charging cases are too aggressive, potentially incurring Li plating. Guided by these simulations, we have chosen 3C CCCV charging protocol for the experimental research in this work.

More simulations to search for the shortest charging time without Li plating at 25°C are shown in Figure 4. With the higher cell temperature, the highest charging current is increased to 5C without causing Li plating.

Results and Discussion

Figure 5a compares SOC evolutions during 3C charging of a 10 Ah ACB cell and a baseline cell without ACB at -30°C , showing that charge time to reach 80% SOC is $11.4\times$ shorter for the ACB cell than for the baseline cell. The total charge time of 14 min for the ACB cell includes 90-sec cell activation to raise the battery core temperature to $\sim 10^\circ\text{C}$. A stark difference in charge acceptance between the ACB

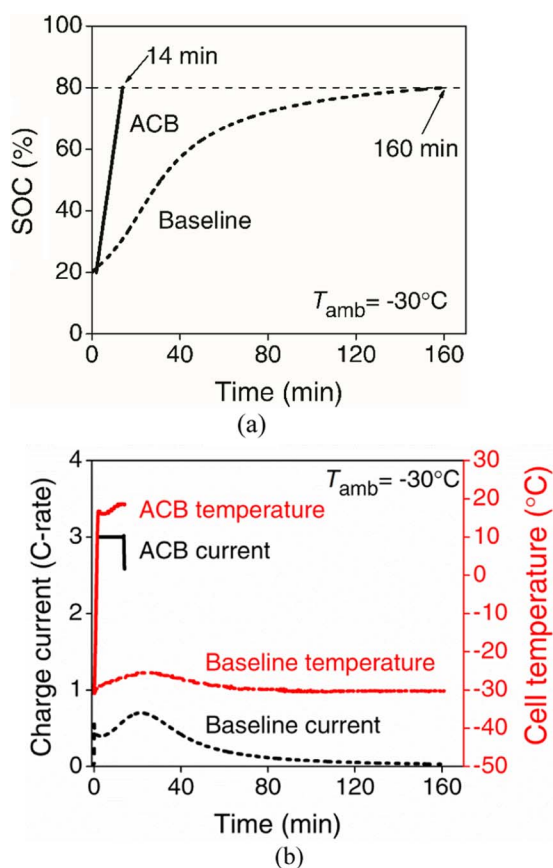


Figure 5. All-weather battery (ACB) vs. a baseline Li-ion cell in charging. (a) State-of-charge (SOC) curves during 3C fast charging (3C, 4.2 V, 80% SOC or C/20 cutoff). The charge acceptance is dramatically increased in the ACB cell after activation for pre-heating, and charging time is improved by 11.4× from the baseline to ACB cell. (b) Temporal evolutions of cell temperature and charge current, showing an order-of-magnitude higher charging current for the ACB cell on average.

and baseline cells can be noted from Figure 5a, ascribing to the fact that the electrode-electrolyte interface in the ACB cell is heated to between 10 and 20°C as shown in Figure 5b. Cell temperature and charge current expressed in C-rate are displayed in Figure 5b for both ACB and baseline cells. The ACB cell temperature is seen to rise rapidly to 10–20°C after 90 sec activation, creating a highly reactive electrode-electrolyte interface for high-rate charging. Indeed, the charge current starts at 3C and remains higher than 2.5C as the ACB cell is charged toward 80% SOC. In contrast, the baseline cell stays around -30°C throughout the entire charge period, resulting in huge overpotential due to sluggish electrode kinetics and ion conduction and hence limiting the charge current (capped at 4.2 V) to only $\sim 0.5\text{C}$ before tapering off to 0.05C. Figures 5a and 5b clearly show that the new ACB structure has dramatically improved charge acceptance of Li-ion batteries in the extreme cold.

Activation of an ACB cell is fundamental to achieving high charge acceptance from low temperatures. This heating process is detailed in Figure 6 for pulse activation from -10°C , -20°C and -30°C . Figure 6a shows that initially at 20% SOC and -10°C , the ACB cell can sustain full pulses, i.e. 3C charge pulse for 1 sec and 5C discharge pulse for 1 sec, without being tapered by the upper and lower voltage limits of 4.2 and 2.1 V. The pulse activation from -10°C lasts for 54 sec when the cell surface temperature reaches the pre-set value of 10°C (Figure 6b). For activation from -20°C and -30°C , some initial pulses are tapered by the upper and lower voltage limits until the cell temperature rises a little higher and the electrochemical interface becomes more reactive. Pulse activation to the pre-set point of 10°C

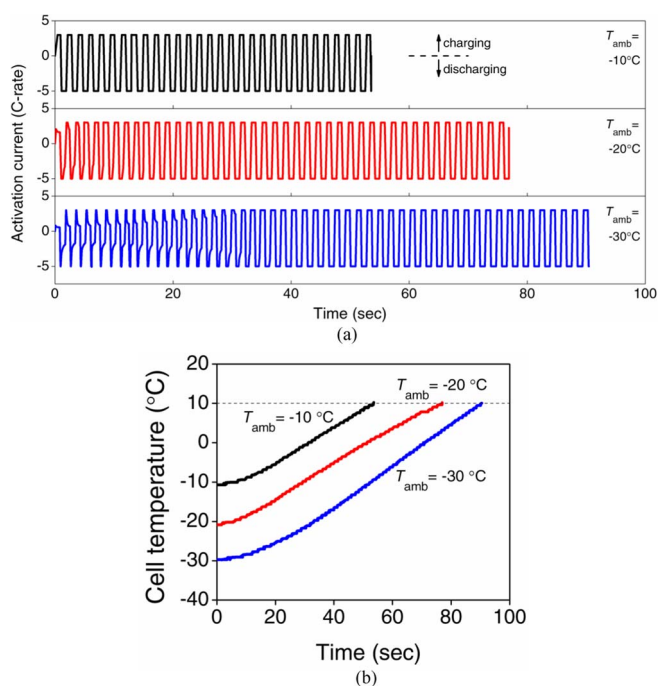


Figure 6. Pulse activation of ACB cell from -10°C , -20°C and -30°C . (a) Activation current profiles, showing short pulses of charge and discharge which do not alter the battery SOC but generate resistive heating internal to the cell. (b) Cell temperature rise with time. Activation time is 54, 77, and 90 sec from -10°C , -20°C and -30°C , respectively. These activation time constants are only small fractions of the total battery charging time.

takes 77 and 90 sec, respectively, for -20°C and -30°C cases. While increasing activation time with decreasing ambient temperature is easily understood, the time necessary for pulse activation still varies only between 6–10% of the total charging time (~ 14 min), demonstrating a super-efficient self-heating method. The waveforms of pulse activation, i.e. discharge/charge current and pulse duration, could be further optimized to speed up the activation process. But more important is to improve the 3C charging process in a self-heated ACB cell, which controls the bulk of the total charging time.

The energy source for internal heating of an ACB cell during activation comes largely from the external charge energy, evident from the battery SOC varying only slightly from initially 20% to 18% at the end of pulse activation. In contrast, in the absence of charge energy, an ACB cell consumes battery energy, e.g. 5.5% of cell capacity for heating from -30°C to 0°C .¹² (More recently, we experimentally demonstrated 2.9% battery energy consumption and 12.5 seconds for self-heating from -20°C to 0°C .¹⁸) Thus, availability of charge energy to internally heat an ACB cell permits to operate ACB cells with any SOC down to zero as well as to develop innovative methods for faster activation. During regenerative braking, the metal foil in an ACB cell, in a sense, acts as an “internal brake” with the great benefit of converting braking energy into thermal energy to warm up battery materials and electrochemical interfaces intimately.

It should be noted that the internal Ni foil heating in the present ACB cell has been compared to existing external heating methods^{19–21} including placement of heating elements outside and between batteries in a multi-battery module.¹² In the latter case, heat must warm up the battery casing before benefiting electrodes and electrolyte inside it, causing low heating speed and high energy consumption. It is generally estimated that for battery heating from -20°C to 0°C , the ACB cell needs 12.5 seconds and 3% battery energy, while external heating methods require ~ 15 minutes and $\sim 10\%$ battery energy. That is, there is ca 50× faster heating speed and 3× more energy efficiency with ACB cells.

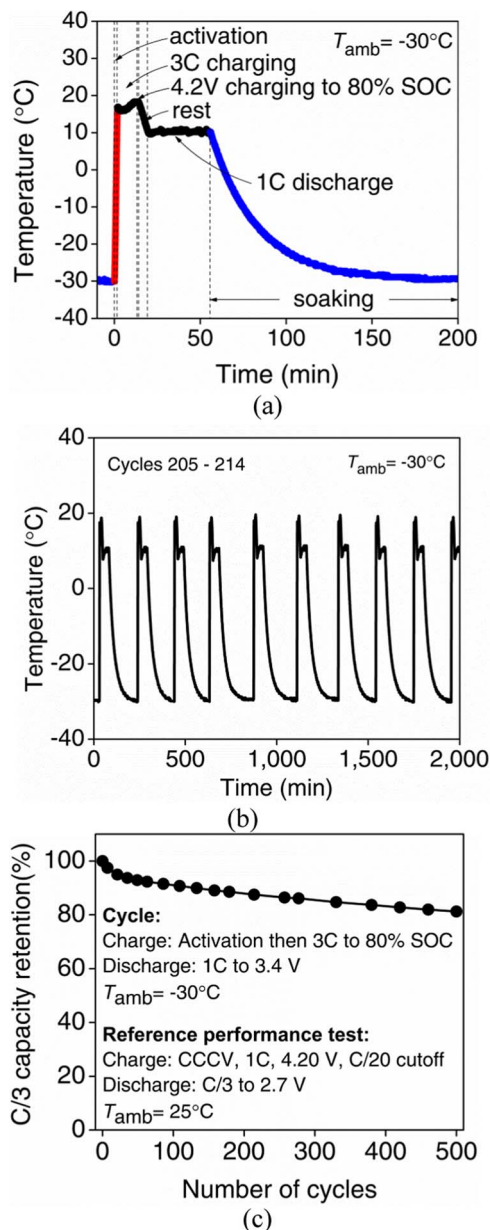


Figure 7. 3C fast-charge cycling from -30°C . (a) Cell temperature evolution within one cycle. Red and blue lines comprise thermal cycling where the heating rate is as high as $26.7^{\circ}\text{C}/\text{min}$ and black lines comprise electrochemical cycling of 3C charge and 1C discharge. (b) Cell temperature profile over 10 cycles, clearly showing the nature of thermal cycling. (c) C/3 capacity retention in percent versus cycle number. The degradation comes from both electrochemical cycling and thermal cycling.

Figure 7 displays experimental results of 3C fast-charge cycling of ACB cell at -30°C . Figure 7a shows the temperature evolution in one whole cycle consisting of pulse activation (90 sec), 3C constant current followed by 4.2 V constant voltage charging until either 80% SOC or C/20 is reached, 5 min rest, 1C constant-current discharge to 3.4 V (corresponding to 20% SOC), and several hours of cell soaking in the -30°C environment at open circuit. Most notable is the rapid rise in cell temperature during pulse activation. Subsequently, the cell temperature stays between 10 and 20°C during the fast charging stage, while it drops to $\sim 10^{\circ}\text{C}$ during rest and 1C discharge due to excessive cooling in the environmental chamber. Finally, the cell is cooled for over 2 hours before reaching thermal equilibrium with the surroundings to start another cycle. The temperature evolution over

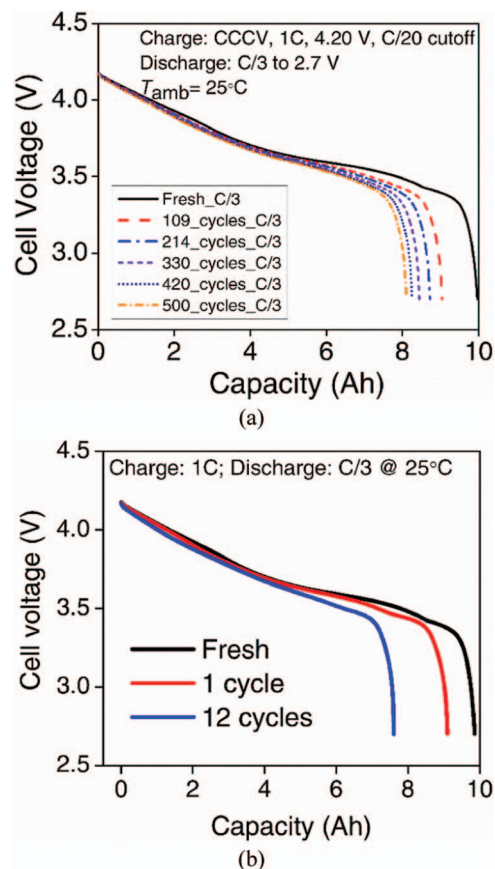


Figure 8. Room-temperature discharge curves of fresh and aged cells from 3C fast-charge cycling at -30°C . (a) ACB cell. (b) Baseline cell.

a series of 10 cycles is shown in Figure 7b, clearly illustrating the simultaneous presence of electrochemical and thermal cycling. At the end of every 20–50 such cycles, the test cell is brought to room temperature and undergoes reference performance characterization. The measured C/3 capacity is plotted in Figure 7c as a function of cycle number. It is seen that the cell capacity retains greater than 80% even after 500 cycles of 3C charging at -30°C . Figure 8a further compares the discharge curves of fresh and aged cells, showing mainly capacity fade plus a modest impedance rise. Assuming 100-mile drive range per charge, 500 cycles shown in Figure 7c are equivalent to 50,000 vehicular miles provided by 3C charging in -30°C extreme cold, clearly demonstrating commercial viability of this activation-charging protocol using ACB cells.

To understand how the ACB cell's fast-charge cyclability at low temperatures as shown in Figure 7 benefits from internal pre-heating, Figure 9a compares the ACB cell's capacity retention with that of the baseline cell fast charged with the same protocol but without activation. It is seen that the cycle number increases from 12 for the baseline cell to 500 for the ACB cell by internal heating that removes the tendency of Li plating. Figure 8b further displays degradation in discharge performance of the baseline cell undergone 3C charge cycling at -30°C . Significant capacity loss due to Li plating is evident after just one charge cycle. The sharp contrast in degradation behaviors of the ACB and baseline cells shown in Figures 8a and 8b demonstrates that thermal stimulation by ACB cell activation effectively minimizes or eliminates Li plating.

The fast-charge cycling protocol described above entails both electrochemical and thermal cycling. The first stage of the ACB cell cycling protocol, i.e. pulse activation to rapidly self-heat a cell (red line in Figure 7a), and the fourth stage, cooling down by forced air convection in the environmental chamber (blue line in Figure 7a),

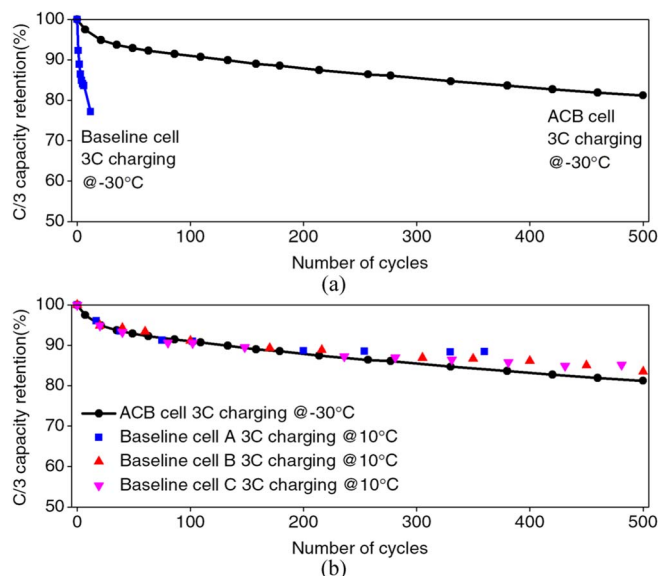


Figure 9. Capacity retention in fast-charging cycles. (a) Comparison in capacity retention of a baseline cell and an ACB cell for 3C charging from -30°C . The cycle life is improved by $40\times$ in ACB cell versus the baseline cell. (b) Capacity retention of ACB cell in 3C charging from -30°C (involving both electrochemical and thermal cycling) and in 3C charging from 10°C (involving electrochemical cycling only).

constitute thermal cycling and involve a rapid temperature swing. On the other hand, the second and third stages (black line in Figure 7a), i.e. 3C charge and 1C discharge, constitute electrochemical cycling at a temperature level of $\sim 10^{\circ}\text{C}$. To differentiate the degradation caused by electrochemical and thermal cycling, we devise another cycling test using a baseline cell cycled with 3C charge/1C discharge at 10°C ambient temperature: 3C, 4.2 V and 80% SOC or C/20 cutoff. This cycling experiment at 10°C closely resembles the electrochemical cycling portion of the ACB cell (the black lines in Figure 7a). The results for a total of three test cells are displayed in Figure 9b to compare with the ACB cell cycling from -30°C , strongly suggesting that the thermal cycling additionally involved in ACB cell's fast-charge cycles has a minimal effect on battery degradation if any. The latter finding is consistent with the capacity retention result from repetitive activation described in Wang et al.¹² In practice, vehicle batteries are thermally insulated and the severity of thermal cycling is far less than that experienced in the -30°C cycling test shown in Figure 9a.

Future efforts could further accelerate the fast charge process at subzero temperatures and reduce charge time from ~ 14 min to 5–10 min without negatively impacting the cycle life. One such solution is to extend the activation period to 25°C so that the highest charging current could be raised to 5C while avoiding Li plating (see Figure 4). In such a scenario, our electrochemical-thermal coupled simulations forecast that the activation time will increase to 125 sec; however the charging time to 80% SOC is reduced to 440 sec under 5C protocol (marked by the red dot in Figure 4), giving a total charge time of 9.42 min. The cell temperature is seen to further rise from 25 to 38°C in this 5C charging process (Figure 4a), after cell activation to raise the cell temperature to 25°C . Experimental verification of such a longer preheating protocol is underway and experimental data shall be reported in a future publication.

Finally, the present model is also applied to simulate pulse activation processes of the ACB cell from -10 , -20 and -30°C , and the predicted and measured temperature evolutions are depicted in Figure 10 with generally good agreement. Thus the model is a useful tool for computational design and optimization of fast rechargeable batteries at low temperatures.

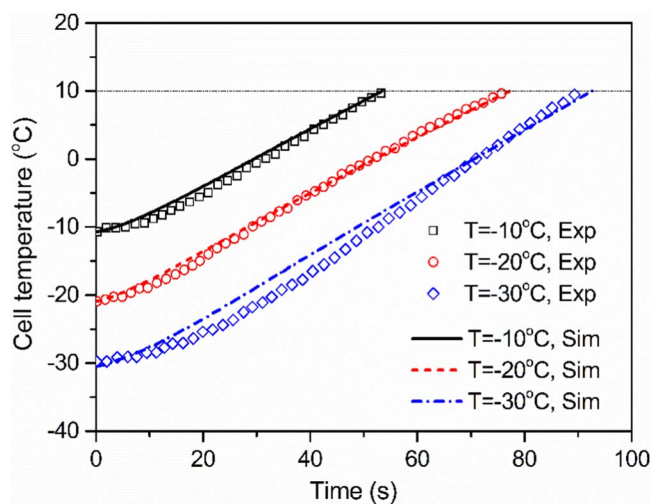


Figure 10. Comparison of predicted (lines) and measured (symbols) temperature evolutions in pulse activation from -10°C , -20°C and -30°C .

Conclusions

We have described an elegantly simple solution to low-temperature charging of Li-ion batteries. We experimentally demonstrated 14-min fast charging to 80% SOC at -30°C with more than 500 cycles without incurring Li plating. Such a finding enables deployment of fast-charging infrastructure to accelerate widespread adoption of PEVs. The ACB technology may also slash battery size and cost for home energy storage with outdoor installation where high-rate charge/discharge at low temperatures is experienced. Grid storage for frequency regulation demands small, inexpensive batteries while providing high-power charge/discharge for 15 minutes.²² Rapid charging is also essential to successful drone fleet delivery. Finally, the fast rechargeable ACB battery at extreme temperatures could critically expand defense and aerospace capabilities. In a broader sense, an ACB cell can be used to quickly and practically transform battery internal states on demand, e.g. trading a tiny fraction of energy for great power (1.5% battery energy will yield 10°C temperature rise and consequently great power boost). We expect this unique battery structure to create a new paradigm for battery science and technology in which important metrics of a battery: energy, power, cycle life and safety, can all be reconfigured and regulated on demand.

Acknowledgments

We acknowledge EC Power for donating AutoLion software licenses to support this work. All-climate battery is the subject of patent protection including U. S. patent publication numbers 2014-0342194, 2015-0303444 and 2015-0104681 and Patent Cooperation Treaty publication numbers WO 2014/186195, WO 2015/102709 and WO 2015/102708.

References

- National Research Council, Overcoming barriers to deployment of plug-in electric vehicles, National Academy of Science, 2015. <http://www.nap.edu/catalog/21725/overcoming-barriers-to-deployment-of-plug-in-electric-vehicles>.
- 120 kW supercharger station from Tesla, <http://www.teslamotors.com/supercharger>.
- 50 kW DC fast charge station for BMW and Volkswagen and ChargePoint, <http://www.chargepoint.com/news/2015/0122/>.
- S. S. Zhang, K. Xu, and T. R. Jow, *Electrochem. Commun.*, **4**, 928 (2002).
- J. Fan and S. Tan, *J. Electrochem. Soc.*, **153**, A1081 (2006).
- M. C. Smart, J. F. Whitacre, B. V. Ratnakumar, and K. Amine, *J. Power Sources*, **168**, 501 (2007).
- F. Orsini, A. Du Pasquier, B. Beaudoin, J. M. Tarascon, M. Trentin, N. Langenhuisen, E. De Beer, and P. Notten, *J. Power Sources*, **76**, 19 (1998).
- Y. Ji, Y. Zhang, and C. Y. Wang, *J. Electrochem. Soc.*, **160**, A636 (2013).
- B. V. Ratnakumar and M. C. Smart, *ECS Transactions*, **25**, 241 (2010).

10. M. Petzl, M. Kasper, and M. A. Danzer, *J. Power Sources*, **275**, 799 (2015).
11. M. Ouyang, Z. Chu, L. Lu, J. Li, X. Han, X. Feng, and G. Liu, *J. Power Sources*, **286**, 309 (2015).
12. C. Y. Wang, G. Zhang, S. Ge, T. Xu, Y. Ji, X. G. Yang, and Y. Leng, *Nature*, **529**, 515 (2016).
13. O. Gröger, H. A. Gasteiger, and J.-P. Suchsland, *J. Electrochem. Soc.*, **162**, A2605 (2015).
14. AutoLion, www.ecpowergroup.com/autolion/.
15. J. Kalupson, G. Luo, and C. E. Shaffer, *SAE Technical Paper*, 2013, 01 (Detroit, MI: SAE International World Congress and Exhibition).
16. M. F. Hasan, C. F. Chen, C. E. Shaffer, and P. P. Mukherjee, *J. Electrochem. Soc.*, **162**, A1382 (2015).
17. Y. Leng and C. Y. Wang, *unpublished research, Penn State University Electrochemical Engine Center*, University Park, PA 16802, 2015.
18. G. Zhang, S. Ge, T. Xu, X. G. Yang, H. Tian, and C. Y. Wang, Submitted for publication.
19. A. Vlahinos & A. A. Pesaran, SAE Technical Paper 2002-01-1975, 2002.
20. T. A. Stuart & A. Handeb, *J. Power Sources*, **129**, 368 (2004).
21. Y. Ji & C. Y. Wang, *Electrochim. Acta*, **107**, 664 (2013).
22. B. Dunn, H. Kamath, and J. M. Tarascon, *Science*, **334**, 928 (2011).